Journal Pre-proofs

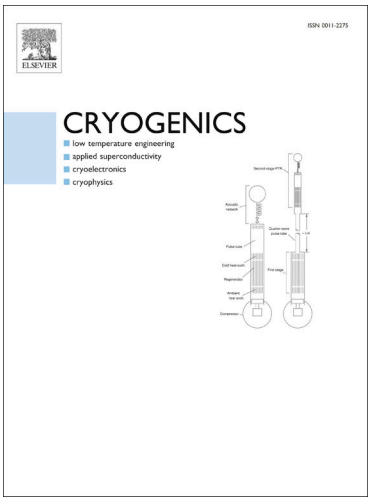

The pressure-volume relationship in an ideal Stirling refrigerator

Danielle Yang, Michael Gschwendtner, Aishath Zindh Waleed, Michael Protheroe

PII: S0011-2275(24)00102-4
DOI: https://doi.org/10.1016/j.cryogenics.2024.103882
Reference: JCRY 103882

To appear in: *Cryogenics*

Received Date: 2 November 2023
Revised Date: 3 May 2024
Accepted Date: 13 June 2024

Please cite this article as: Yang, D., Gschwendtner, M., Waleed, A.Z., Protheroe, M., The pressure-volume relationship in an ideal Stirling refrigerator, *Cryogenics* (2024), doi: https://doi.org/10.1016/j.cryogenics.2024.103882

The Pressure-Volume Relationship in an Ideal Stirling Refrigerator

Danielle YANG*, Michael GSCHWENDTNER, Aishath Zindh WALEED, Michael PROTHEROE
Auckland University of Technology, 55 Wellesley St E, Auckland, New Zealand

*Corresponding author: danielle.yang@aut.ac.nz

Abstract

Hysteresis losses in the heat transfer between compressing or expanding gas and the adjacent wall is said to play an important role in Stirling machines, where it increases the amount of required p-V work. Previous studies have linked hysteresis loss with the pressure phase shift. In the context of this research, the effect of the pressure phase shift on the net p-V work in a single space is examined.

A Sage model of a single space piston-cylinder device is used to investigate the underlying mechanisms of the pressure phase shift. The Sage model is validated using an experimental piston seal rig. In addition, the time dependence of heat transfer is discussed along with how it affects the pressure phase shift, using an iterative model. The Schmidt equations were manipulated to determine the phase shift between pressure and volumetric oscillation in an ideal Stirling refrigerator.

The results of this investigation are surprising. It was found that even in the case of an idealized Stirling refrigerator, the phase shift between pressure and volume is non-zero in order to produce a refrigeration effect.

1 Introduction

Stirling coolers consist of several spaces in which a volume of gas undergoes expansion and compression. As the gas goes through these cyclic compression and expansion processes, heat is transferred to and from the cylinder walls and the working gas, and the result is a net heat transfer out of the working gas. Net heat transferred from the gas to the walls increases the required p-V work input, as the compression work input is larger than the recovered expansion work (Scheck, 1988). This cyclic heat transfer from the gas to the walls, resulting from heat transfer processes associated with oscillating pressure and volume in a gas system, is known as hysteresis loss.

Hysteresis loss is a hardly understood phenomenon, associated with an efficiency loss in Stirling engines and refrigerators. It has been suggested that a Stirling engine typically loses 5% of its output power to thermal hysteresis but can lose up to 25% if the engine is small and operates at high frequencies (Scheck, 1988). Some do not quantify it, but rather state that it is a large or important thermal loss (Lee, Smith, & Faulkner, 1980), and do not offer a conclusion on its effect, but state that existing methods are either sufficient (Kornhauser, 1989; Kornhauser & Smith, 1987; Kornhauser & Smith, 1993; Pourmovahed & Otis, 1984) or insufficient (Wang, 1988; Willich, Markides, & White, 2017) in determining its magnitude. Furthermore, yet another study concludes that hysteresis loss is negligible (Park & Chang, 1997). In addition, the pressure phase shift is understood to be one of the key factors in the magnitude of hysteresis loss (Kornhauser, 1989; Kornhauser & Smith, 1993; Scheck, 1988; Yang & Gschwendtner, 2018).

The purpose of this study was to contextualise how hysteresis loss fits within our current understanding of net work input into the Stirling refrigerator. To investigate if the pressure phase shift is an inherent mechanism of the work-heat relationship or an indicator of the magnitude of heat transfer losses, all other phenomena such as friction losses, dead volume, and multiple spaces are excluded from the analysis.

1.1 Stirling Refrigerators

The Stirling cycle is a regenerative gas cycle. One of the main advantages of these machines over the conventional vapour-compression heat pumps and refrigerators is that Stirling machines operate on environmentally friendly working gases such as air, helium, and hydrogen (Walker et al., 1994). They have been used as heat engines for power generation in co-generation plants, in waste heat recovery, and in space applications.

As a refrigerator, Stirling technology has been used in cryo-cooling and lab freezer applications. Stirling machines have been recognised to hold the potential for commercial competition to the vapour-compression refrigerators and heat pumps currently in widespread use, but as of today, they have not been able to successfully break into the large markets of industrial and home refrigeration (Haywood, 2004; Walker et al., 1993, 1994; West, 1986; Wurm et al., 1991). They have, however, been effective in niche areas such as cryo-cooling for medical and laboratory applications (Stirling Ultracold, 2018; Urieli & Berchowitz, 1984).

1.2 Stirling Cycle Modelling

There has been an incredibly wide range of mathematical models developed in the attempt to predict Stirling machine performance or to specify beneficial design criteria. They vary from the simple to the complex due to a multitude of different factors, which includes the assumptions available, the solution method used, their degree of realism and so on (Chen & Griffin, 1983; Martini, 1983; Urieli, 1983).

The ideal Stirling cycle is traditionally modelled using discrete piston motion to describe the cycle's isochoric and isothermal processes. During the isothermal processes, the working gas is either compressed or expanded, and heat flows in or out of the cycle. During the isochoric processes, heat is internally transferred by the regenerator by alternately absorbing and rejecting heat into the working gas.

Practical Stirling refrigerators usually use sinusoidal or near-sinusoidal motion of their pistons to move gas between the hot and cold spaces. Possibly one of the most well-known models within the Stirling community is the analysis by Gustav Schmidt published in 1871 (Schmidt, 1871). This simple first-order model takes into consideration sinusoidally varying working

spaces and assumes isothermal heat transfer. It takes into consideration the expansion and compression space volume separately and assumes that the heat exchangers and regenerator are ideal and contribute to the total dead volume of the system.

The derivation of the following parameters can be found in Walker's (1983) comprehensive text on cryocoolers. The Schmidt cycle model assumes that the expansion and compression spaces vary sinusoidally with the swept volumes being $V_{E,swept}$ and $V_{C,swept}$. The ratio of these swept volumes is $\kappa = \frac{V_C}{V_E}$, while the volume variation of the expansion space leads that of the compression space by the phase angle, β, and the crank angle is θ, which varies from 0 to 360°, or from 0 to 2π. The volume variation in the expansion and compression space are defined in Equations 1 and 2.

Cyclic volume variation of the expansion space:

$$V_E = \frac{1}{2} V_{E,swept}(1 + \cos(\theta)) \qquad \text{Equation 1}$$

Cyclic volume variation of the compression space:

$$V_C = \frac{1}{2} V_{C,swept}(1 + \cos(\theta - \beta)) = \frac{1}{2} \kappa V_{E,swept}(1 + \cos(\theta - \beta)) \qquad \text{Equation 2}$$

The temperature ratio is the ratio of the compression space temperature to the expansion space temperature, $\tau = \frac{T_C}{T_E}$.

The minimum and maximum pressures in the cycle are at:

$$\theta_{P_{min}} = \phi = \tan^{-1}\left[\frac{\kappa \sin(\beta)}{\tau + \kappa \cos(\beta)}\right] \qquad \text{Equation 3}$$

and

$$\theta_{P_{max}} = \theta_{P_{min}} + \pi \qquad \text{Equation 4}$$

Looking at Equations 1 through to 4, it can be seen that the Schmidt model does not explicitly give the phase shift between the overall volume wave and the pressure wave. The pressure phase shift is an important quantity in the study of hysteresis loss. The Schmidt equations are extended in Section 5 to derive the pressure phase shift for an ideal sinusoidal Stirling refrigerator.

1.3 The Pressure Phase Shift

As discussed by Chafe (1988), Kornhauser and Smith (1987), in an ideal single piston-cylinder device with no heat transfer, the pressure and volume waves are exactly 180° out of phase. To clarify conventions, Figure 1-1 shows pressure and volume as sinusoidally varying normalised functions. The pressure phase shift is defined by how much the actual pressure leads the ideal pressure wave. This can also be seen in Figure 1-1, which shows how an increasing phase shift, ϕ, affects the pressure wave.

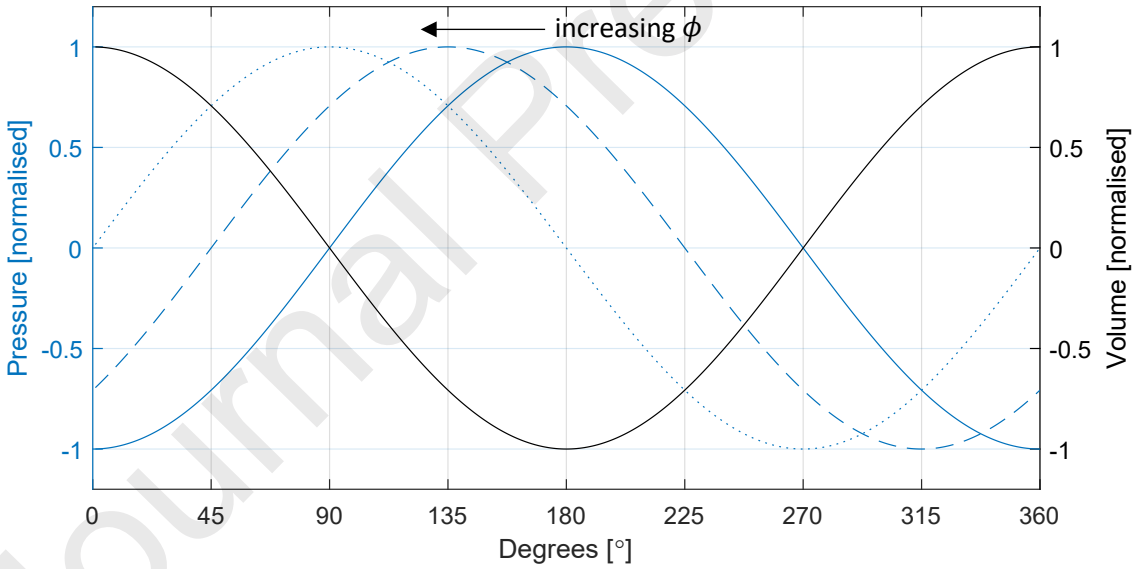

Figure 1-1: Volume and pressure as sinusoidally varying functions with an increasing pressure phase shift, $\boldsymbol{\phi}$

Literature has shown that the net p-V work input and pressure phase are intrinsically linked. They both are low at both extremes of low and high operating frequencies and have a peak between the two at similar frequencies. This indicates a connection between the pressure phase shift and the net p-V work (Chafe, 1988; Kornhauser, 1989; Kornhauser & Smith, 1987; Kornhauser & Smith, 1993; Scheck, 1988; Yang & Gschwendtner, 2018). In Kornhauser's 1989

experiments, this phase shift ranged from approximately 0.5 to 12 degrees. What remains to be studied is the relationship between the two – is it possible to have net p-V work with no pressure phase shift, and vice-versa?

1.4 Objectives of the Study

This study's objective is to understand the underlying mechanisms of the pressure phase shift in a single cylinder device using a range of different tools. Initially, a Sage model of a single space piston-cylinder device was created. It was run to see how p-V work, pressure, temperature, and heat transfer changes over the cycle as the frequency of oscillation increases. This was to understand how these properties change for different modes of operation – isothermal at low frequencies, transition at intermediate frequencies, and adiabatic at higher frequencies. The Sage model was also experimentally validated using a piston-seal test rig in Section 4. In addition to the Sage model, an iterative transient heat transfer model was produced to demonstrate the fundamental relationship between heat transfer and the pressure phase shift.

After studying what causes the pressure phase shift, the pressure phase shift is defined in existing models, in order to explain the relationship between the pressure phase shift and the net p-V work. For sinusoidal piston motion, an equation relating the pressure phase shift and the net p-V work is established for a single space. This formed the basis of understanding the overall system. After this, the pressure phase shift was found when applied specifically to Stirling refrigerators. The Schmidt equations are then used for this analysis, by re-arranging the Schmidt equations to find the total volume wave and the pressure phase shift.

2 Single Cylinder Sage Model

Sage is a numerical software package for Stirling machines, developed by David Gedeon (Gedeon, n.d.). It contains a library of different components whose properties, inputs, and dimensions can be defined by the user. These components are all joined by connections that model flows such as heat flow, mass flow, force, and pressure (Gedeon, 2016). Sage can model heat transfer processes and fluid friction of oscillating flow – even through porous media such as the regenerator matrix. Each component of the system is analysed in a one-dimensional form subdivided into a user-defined number of spatial increments.

Sage applies a variation of the three basic momentum, continuity, and energy equations to each control volume. They are not in the standard form as they are designed specifically for one-dimensional internal flows with space- and time- variable flow area (Gedeon, 2016). The starting integral form equations are listed below in Equations 5-7. In these equations, the control volume, v, is fixed only at the inlet and exit boundaries, but considers moving side boundaries which consist of time-variable flow areas. However, these side boundaries are impermeable so that flow only enters and leaves through the inlet and exit boundaries.

Continuity: $$\frac{d}{dt}\int_v \rho dv + \int_s \rho n \boldsymbol{V_r} ds = 0 \qquad \text{Equation 5}$$

Momentum: $$\frac{d}{dt}\int_v \rho \boldsymbol{V} dv + \int_s [(n\boldsymbol{V_r})\rho \boldsymbol{V} - n\boldsymbol{\sigma}] ds = 0 \qquad \text{Equation 6}$$

Energy: $$\frac{d}{dt}\int_v \rho e dv + \int_s n(\rho e \boldsymbol{V_r} - \boldsymbol{\sigma V} - \boldsymbol{q}) ds = 0 \qquad \text{Equation 7}$$

where $e = \varepsilon + u^2/2$ (the mass-specific total gas energy), $\boldsymbol{n}$ = unit outward normal of s, $\boldsymbol{q}$ = heat flux vector, t = time, v = control volume, $\boldsymbol{V}$ = Newtonian-frame flow velocity vector, $\boldsymbol{V_r}$ = boundary-relative flow velocity vector, ε = mass-specific internal gas energy, ρ = gas density, and $\boldsymbol{\sigma}$ = stress tensor.

A Sage model of a simple piston-cylinder device, with its physical representation shown in Figure 2-1 and Sage interface in Figure 2-2, was created to investigate how pressure, temperature, heat transfer, and p-V work are correlated. This model is validated against experimental results in Section 3.

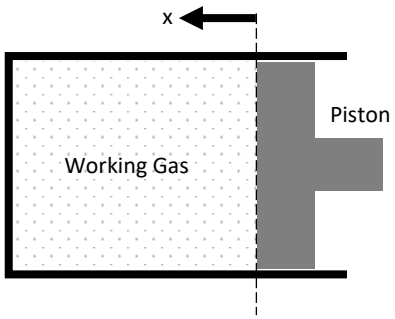

Figure 2-1: Piston-cylinder schematic

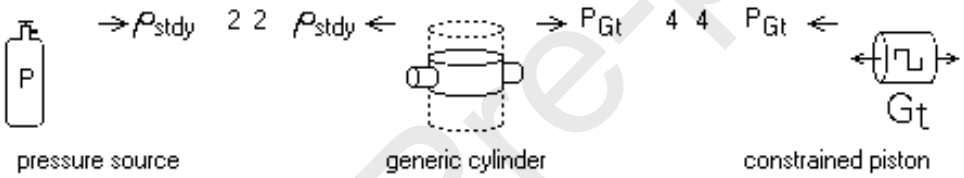

Figure 2-2: Sage model of piston-cylinder experiment

The cylinder wall was modelled as a 'thick surface', which has two layers: a thermally large cylinder wall layer, held constant at a temperature T_w = 300 K to simulate room temperature surroundings, and a thin layer on its surface with a time-varying heat flux, adjacent to the working gas.

The results of the pressure phase shift and the net p-V work for the Sage single cylinder model are shown in Figure 2-3. The pressure phase shift and the net p-V work input are low at both extremes of low and high operating frequencies and have a peak between the two at very similar frequencies. In addition, Figure 2-4, shows the net heat and p-V work against the operating frequency – as expected, for a simple piston-cylinder device, the net p-V work is equal to the net heat transfer output by the system for all frequencies.

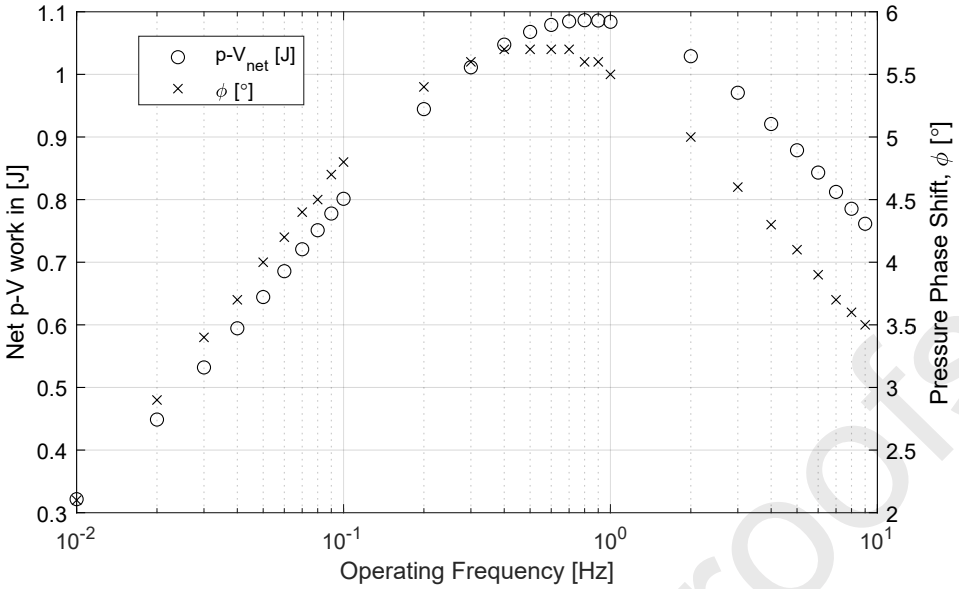

Figure 2-3: Net p-V work and pressure phase lead vs operating frequency for piston-cylinder Sage model

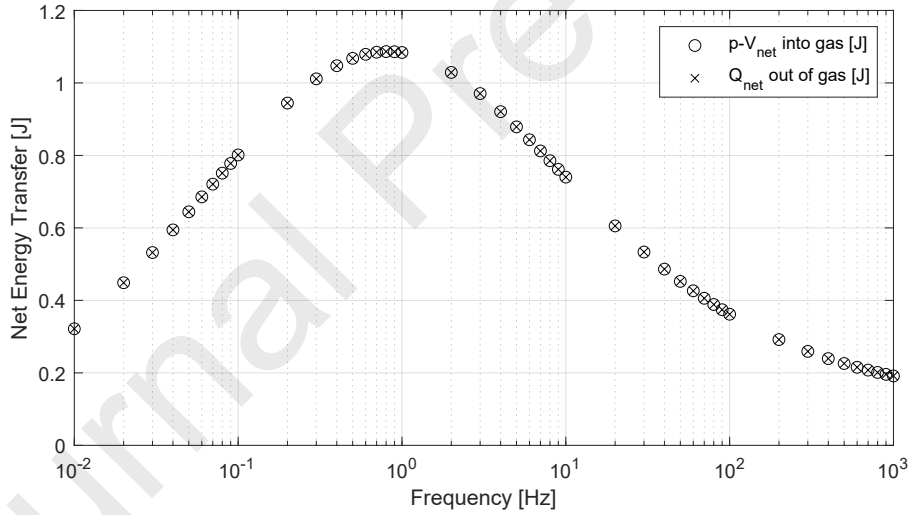

Figure 2-4: Net heat transfer and p-V work against the operating frequency

The instantaneous heat output over one cycle from the gas, and p-V work input for low, medium, and high frequencies (0.01, 0.9, and 10 Hz) are shown in Figure 2-5. The Sage results of the single space model which are closest to isothermal heat transfer can be seen in Figure 2-5. This shows that for low frequencies, the instantaneous heat output is almost identical to the p-V work input. It is not quite perfectly isothermal as the heat output wave is slightly lower in magnitude and has a small lag on the p-V work.

As the operating frequency increases, the instantaneous heat transfer starts to lag the p-V work input due to the decreasing time available for heat transfer, while the heat transfer amplitude decreases. As the operating frequency increases towards adiabatic, the heat transfer amplitude is small (truly adiabatic heat transfer, the heat transfer amplitude would be zero) and the phase lag is large.

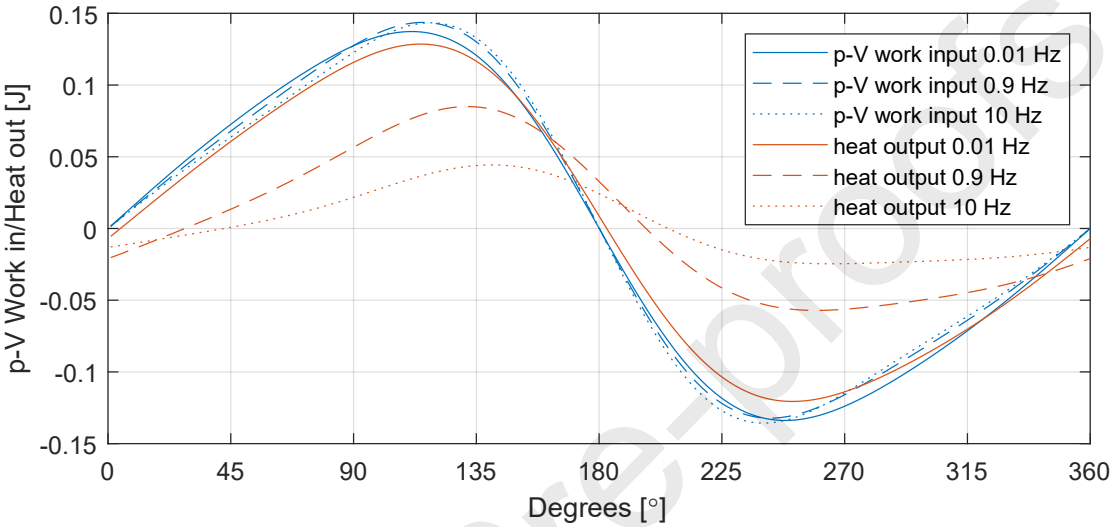

Figure 2-5: Cyclic heat transfer and p-V work for 0.01 Hz, 0.9 Hz, and 10 Hz

2.1 The Mechanisms of the Pressure Phase Shift

How is the pressure phase shift connected to both heat transfer and net p-V work? Understanding them with respect to the fundamental equations of the first law and the ideal gas law leads to a simple explanation. Firstly, consider the two ideal cases at infinitely low and infinitely high operating frequencies. Isothermal heat transfer occurs at slow operating frequencies, so that there is enough time that the temperature, and therefore the internal energy of the gas, to remain constant as the gas is compressed and expanded. This can be seen in Figure 2-6. There is no temperature difference developed between the gas and the wall, so there will also be negligible net gas-wall heat transfer.

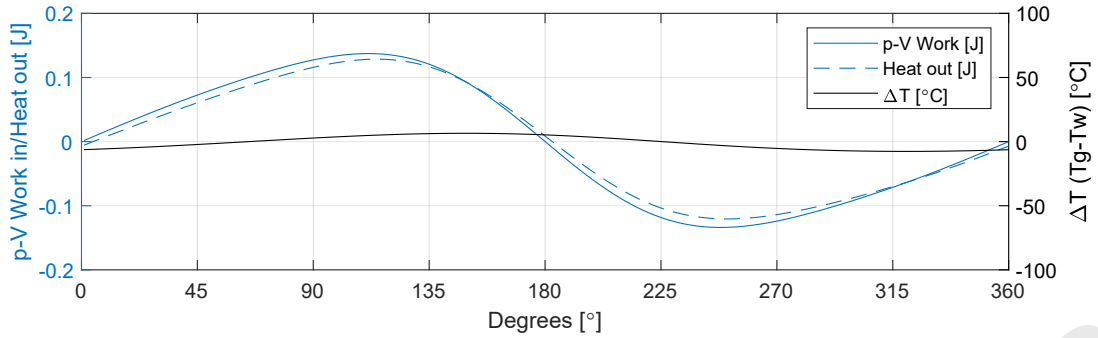

Figure 2-6: Cyclic p-V work, heat transfer and temperature difference at 0.01 Hz

Adiabatic operation would occur at high frequencies, so there would not be enough time for heat to transfer between the gas and the cylinder walls. All the p-V work into the system is converted into a change in internal energy, and therefore there is a large temperature increase in the gas, as seen in Figure 2-7. However, due to the time required for heat transfer, even though there is a temperature difference developed between the gas and the wall, there is negligible net heat out of the gas.

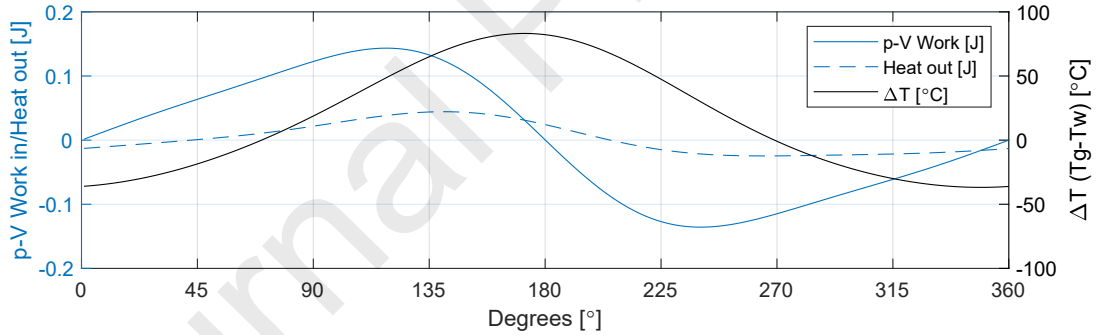

Figure 2-7: Cyclic p-V work, heat transfer and temperature difference at 10 Hz

For both extreme processes, the pressure phase shift is zero, and so is the net p-V work. A zero value for net p-V work makes sense for both these scenarios. This follows from the first law: for both isothermal and adiabatic processes, the net heat transfer over each cycle is zero. For isothermal processes, this is due to complete conversion between heat and work, and for adiabatic processes this is due to insufficient time for heat transfer, resulting in the work being completely converted to internal energy. Following the first law, as there is no net heat

transfer out of the system, the net p-V work transfer into the system is also zero. This was shown in Figure 2-4 where, taking the working gas as the control volume, the net heat out and net p-V work input are equal and opposite.

When the heat transfer characteristics fall in between the two extreme processes, the input p-V work is "distributed" between the change in internal energy and the heat transfer out of the gas, so the full first law applies:

$$\oint Q + \oint W = \oint dU \qquad \text{Equation 8}$$

The quantities affecting the pressure of a closed system are the volume and temperature of the gas, as outlined in the ideal gas equation of state:

$$P = \frac{mRT}{V} \qquad \text{Equation 9}$$

Where P = gas pressure (Pa), m = gas mass (kg), R = universal gas constant $\left(\frac{J}{molK}\right)$, T = gas temperature (K), and V = gas volume (m^3).

Since the volumetric change is specified by the piston motion, it must be the temperature that affects the pressure variation. During the compression process, the temperature of the gas increases to be higher than that of the adjacent walls, which causes gas-to-wall heat transfer, decreasing the internal energy (and therefore temperature) of the gas before the piston reaches the top dead centre. This decrease in temperature also causes the pressure to drop before the top dead centre – this lead is the pressure phase shift. Figure 2-10 is used to illustrate this concept. As the bulk of the heat transfer out of the gas occurs at the end of the compression process, pressure and temperature of the gas are high during compression. Subsequently, the pressure is lower during the expansion process than it would have been, had there not been heat transfer out of the gas during the compression process.

Because of the aforementioned process, not all the compression work is recovered during expansion, and there is a net p-V work input required which is equal to the net heat lost. It is therefore no surprise that the maximum phase shift of the pressure wave coincides with the

p-V work in terms of the frequency, as seen in Figure 2-3. The following sections detail the verification of this Sage model using experimental data.

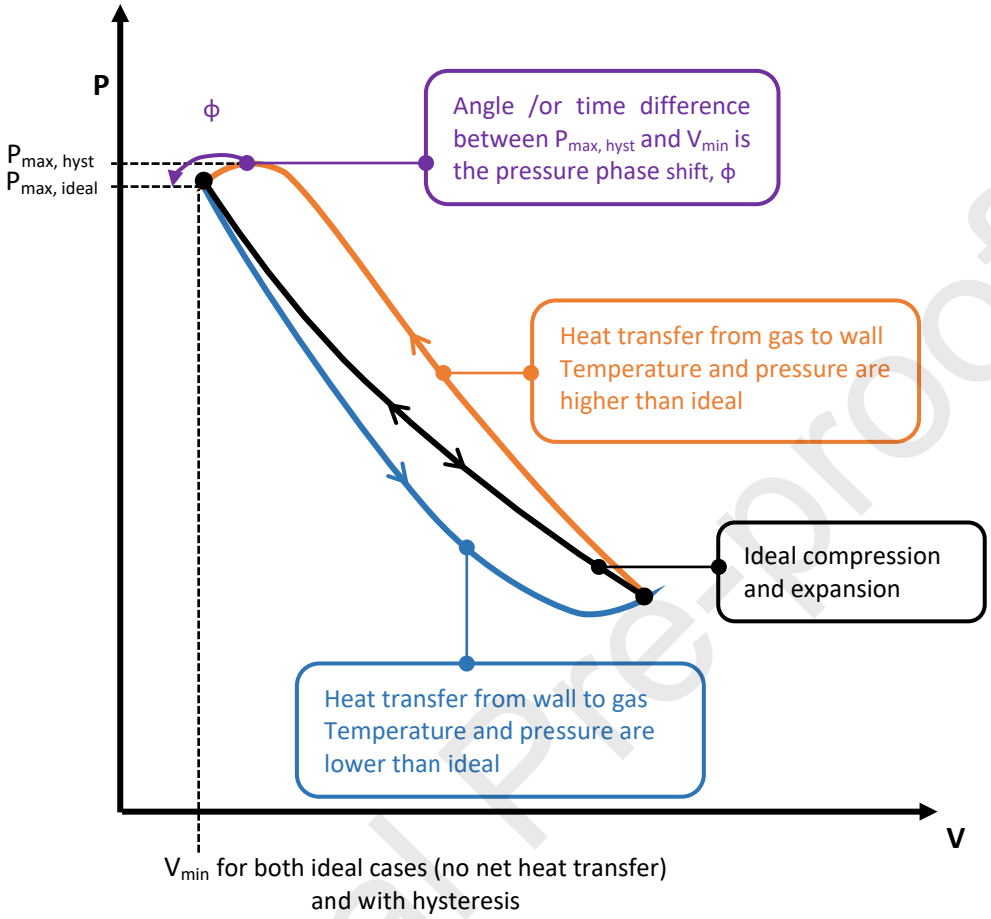

Figure 2-8: p-V diagram showing pressure phase shift

3 Experimental Validation of Sage Model

An existing single cylinder piston seal test rig was used to obtain experimental results to validate the Sage model in Section 2. The entire setup can be seen in Figure 3-1. This includes, from left to right, a) the laboratory computer running LabVIEW, b) the National Instruments (NI) myRIO, the c) H-Bridge, the d) piston-cylinder test rig, and e) the power supply. The NI myRIO is a reconfigurable input/output device which was used for data acquisition, and the H-Bridge controlled the voltage polarity to the linear motor driving the piston.

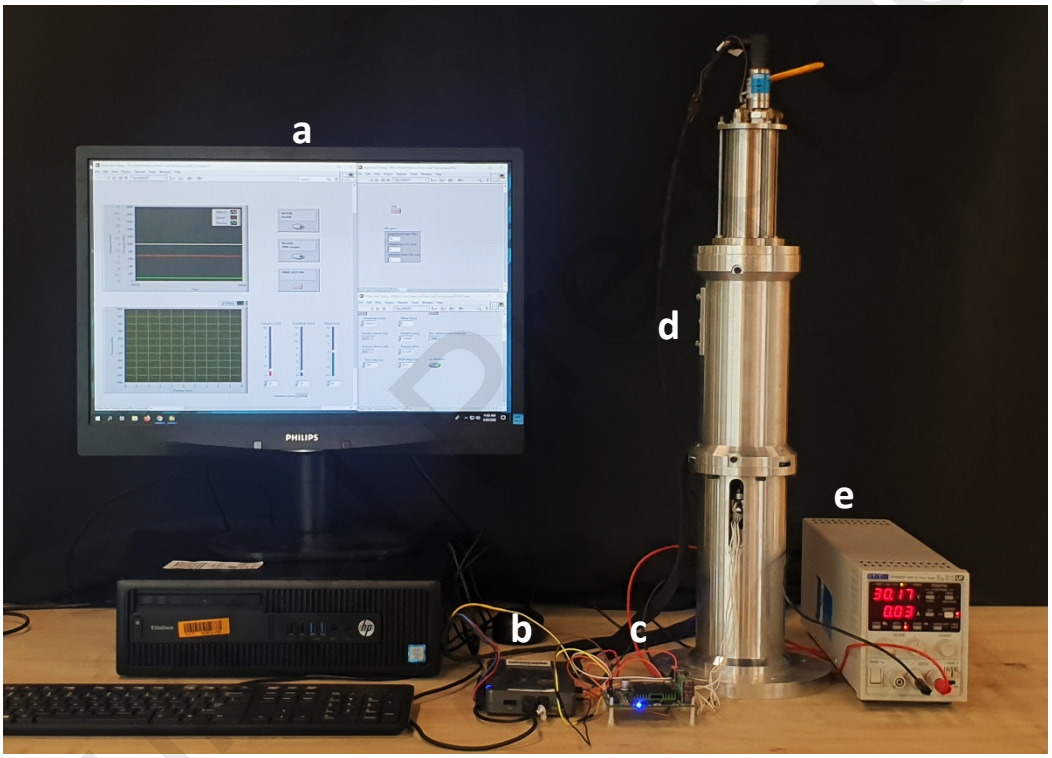

Figure 3-1: Single cylinder test rig set up

The test rig consisted of a modular stainless-steel cylinder with a removeable head, and a piston driven by a moving coil linear motor, supported by flexure bearings. The test rig stood vertically, with the linear motor housing at the base, with the piston shaft going through a middle section with the flexure bearings, and with the piston-cylinder housing at the very top. The test rig had a ball valve which could be opened and closed to allow pressure equalisation with the surroundings. As the test rig was vented to the surroundings, the working gas was air. The piston was sealed with a Viton O-ring which was lubricated with a very thin oil film.

The labelled cross-sectional view of the piston-cylinder test rig is shown in Figure 3-2. The actual working gas space is a small part of the setup, located at the very top. The flexure bearings ensure that the movement is confined to the axial direction, as they have low axial stiffness and high radial stiffness. Relevant dimensions of the test rig are detailed in Table 3-1.

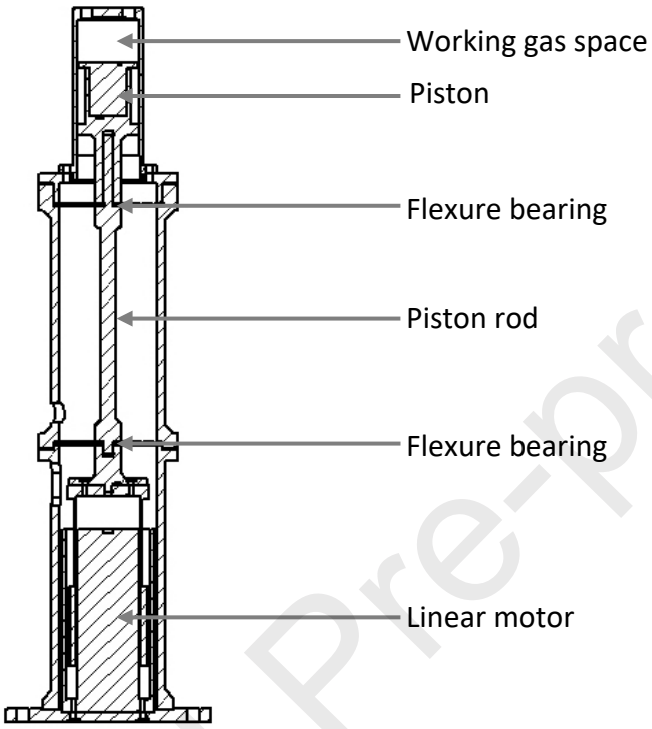

Figure 3-2: Single cylinder test rig labelled cross sectional view

Table 3-1: Piston-cylinder test rig model dimensions

Parameter	**Value**	**Unit**
Diameter	0.05	m
Stroke	0.01	m
Stroke Volume	1.9634×10^{-5}	m^3
Volume Ratio (Compression Ratio)	1.5178	
Average Volume	4.775×10^{-5}	m^3
Piston Face Area	7.854×10^{-3}	m^2
Average Wetted Surface Area	7.747×10^{-3}	m^2
Hydraulic Diameter	2.465×10^{-2}	m

Gas pressure and piston position were recorded to compare with Sage model results of the single cylinder experiment. These results were then processed into their respective physical pressure and position units and written to files through LabVIEW.

The pressure data was recorded using an IPS Series Industrial Pressure Sensor number 7974970, a piezo-resistive thick film ceramic sensor with a stainless-steel body. The pressure sensor full scale range is -1 bar to 9 bar, corresponding to 0 to 5 VDC. The accuracy of the pressure sensor is stated to be less than ± 0.25 % of the full-scale output range.

The position data was recorded using a Honeywell SMART 35 mm Position Sensor, which consisted of an array of magnetoresistive sensors combined with an application-specific integrated circuit to determine the piston position within a magnetic field. This position data was also used as the feedback in the control of the piston. The full-scale range is 0 mm to 35 mm, corresponding to 0.55 and 4.14 VDC. The linearity of this sensor is ± 1.0 % of the full-scale output range.

3.1 Experimental Method

The piston motion was controlled via LabVIEW using closed-loop proportional control. The amplitude of the piston was not able to be accurately set as the piston was not able to reach the full amplitude of the control signal. To compensate for this, the amplitude control was set higher than the required amplitude in order for the piston to reach the required amplitude. It was found that the discrepancy between the control amplitude and actual piston amplitude was around 2-3 mm.

Each experimental sample of pressure and position was taken in real time over one second in millisecond increments, after waiting for just enough time for the position signal to stabilise. The experiment was run in steps of 1 Hz from 1 to 10 Hz. For each frequency, 5 - 10 experimental data sets were taken, and the data set closest to 5 mm amplitude was used while the rest were discarded. This was to ensure that the swept volume was kept as consistent as possible.

3.2 Experimental Results

To compare the experimental results with the Sage model results, the pressure amplitude data was normalised against the respective mean pressures, and the Sage mean volume for each frequency was changed to match the experimental mean volume.

The single cylinder Sage model was set up to replicate the experimental test rig, using air as the working gas and dimensions as outlined in Table 3-1. It was run in steps of 1 Hz, from 1 to 10 Hz, with the mean pressure and volume as an input from the experimental readings for each frequency step. The normalised pressure results for both the single cylinder test rig and its Sage model are displayed in Figure 3-3. The error of the pressure reading is ± 0.25 % of the full-scale range, and this error was also normalised against the mean pressure to show the experimental error range and where the Sage values fall in respect to these error ranges.

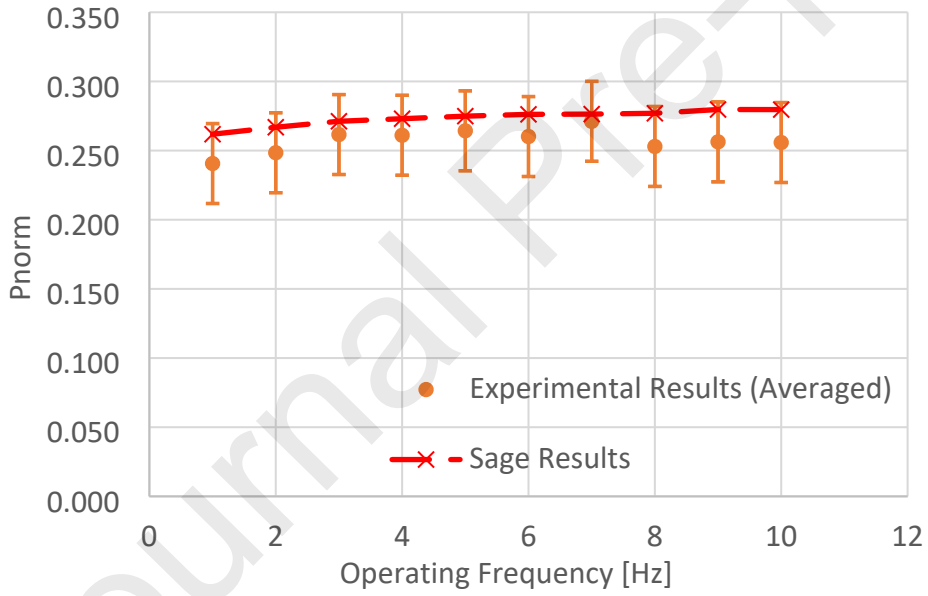

Figure 3-3: Experimental and Sage normalised pressure vs operating frequency for single space piston-cylinder experiment

The Sage-calculated results follow the experimental data very well, although the Sage data is systematically higher than the experimental values. This can be due to seal leakage losses within the experiment, and heat flow from the gas into the piston head or other parts of the experiment that are not modelled in Sage, which would lead to a lower than theoretical pressure amplitude. While Sage considers losses such as seal leakage and shuttle heat

transfer, and the experiment has even more losses still, all which will contribute to the pressure-volume relationship, it is helpful to also understand the fundamental relationships between heat transfer and the pressure phase shift without all other effects. This was done using a simpler model, the transient heat transfer model, which used only a transient heat transfer equation, the first law, and the ideal gas equation.

4 Transient Heat Transfer Model

An iterative or 'step' model for single space heat transfer was developed to demonstrate the interdependency of heat transfer and the pressure phase shift, without losses such as shuttle heat transfer or piston seal leakage. This model was set up in MATLAB – the cycle was divided into 360 degrees, which gave the change in volume for each step. The resulting end properties of each step were calculated using the method shown in Figure 4-1, and the cycle was calculated again until the cycle reached a steady state condition.

Heat transfer from the gas to the cylinder walls was modelled as if the walls were a semi-infinite body: a single plane surface which extends to infinity, with constant thermophysical properties, of which heat transfer only affects the temperature variation near the surface. The equation for the heat transfer was based on a constant surface temperature, T_s, at the surface for $x = 0$, where x is the perpendicular distance into the wall. The formulation for heat transfer as per Bird, Stewart and Lightfoot (1960) and Carslaw and Jaeger (1959) is described as follows:

Differential equation: $$\frac{\partial^2 T}{\partial x^2} = \frac{1}{\alpha} \frac{\partial T}{\partial t}$$ Equation 10

Boundary conditions: $T(0,t) = T_s$ and $T(x \to \infty) = T_i$ Equation 11

Initial condition: $$T(x,0) = T_i$$ Equation 12

The resulting heat flux equation is shown in Equation 13, determined from Fourier's law.

$$\dot{q}(t) = \frac{k(T_s - T_i)}{\sqrt{\pi \alpha t}} \qquad \text{Equation 13}$$

Where k = thermal conductivity of the wall $\left(\frac{W}{mK}\right)$, T_s= surface temperature (K), T_i = initial gas and wall temperature (K), α = wall thermal diffusivity $\left(\frac{m^2}{s}\right)$, and t = time taken for heat transfer (s).

The heat flux equation (Equation 13) was applied in a simple model programmed in MATLAB. The model was based on a specified sinusoidal variation in a volume of working gas, discretised into steps. Properties such as temperature, pressure, and the change in internal energy were initialised for the first step and then were subsequently calculated for each volumetric change. In order to apply Equation 13 in this model, it was multiplied by the instantaneous surface area of the cylinder in direct contact with the volume-changing working gas, A_s, and the change in time for one time step, Δt, to obtain Equation 14, the amount of heat transfer in Joules for one incremental change in volume, ΔV. The variable Δt replaces t in the denominator as the time taken for heat transfer is the same given for one time step:

$$q(t) = \frac{kA_s(T_s - T_i)}{\sqrt{\pi \alpha dt}} \Delta t \qquad \text{Equation 14}$$

The solution process is shown in Figure 4-1. This shows the equations used to calculate all the properties for one volumetric step. For each step, an isentropic temperature change is assumed from T_{n-1} to T_{isn} as the volume changes from V_{n-1} to V_n. The isentropic assumption is used only as an initial estimate for the temperature change, for which heat transfer can be estimated using Equation 14 and using $T_{isn} = T_n$. The work input is calculated using the assumption that $W_n = P_{n-1}\Delta V$, and the change in internal energy, ΔU_n,

is calculated using the first law. The working gas used was helium, and the wall material used was SS304.

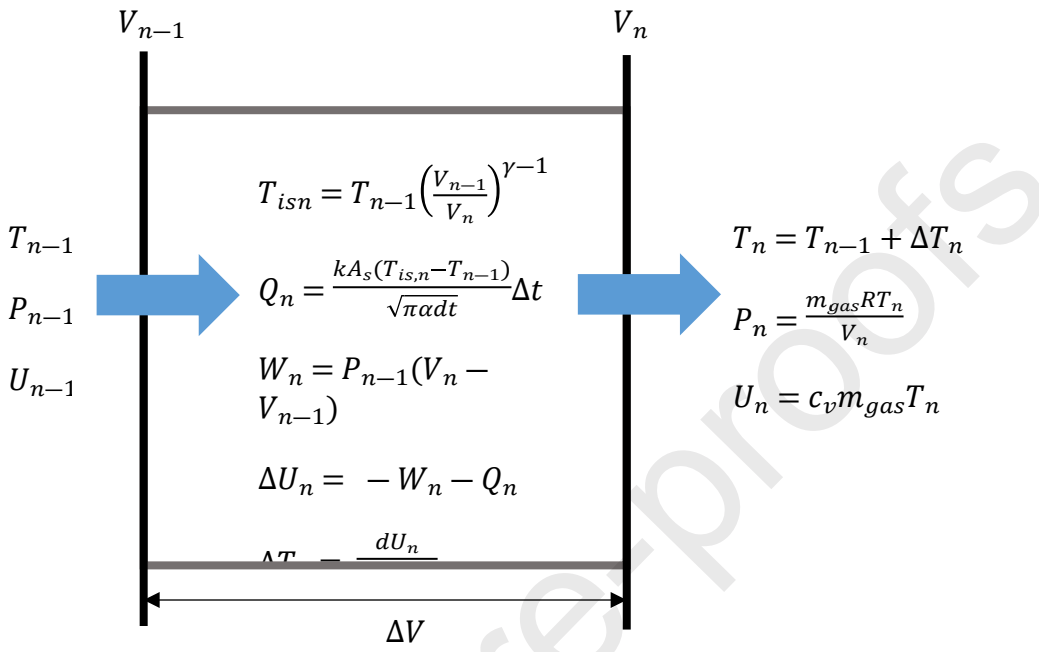

Figure 4-1: Solution process for one volumetric step in the transient heat flow step model

Adiabatic, polytropic, and isothermal results for temperature and pressure were also calculated with the step model. For the adiabatic step model results, the heat transfer was set to zero. This results in all the p-V work being transferred to the internal energy of the gas. In the isothermal model, the change in internal energy was set to zero.

The polytropic results were calculated slightly differently as both pressure and temperature of the next step could be defined with the polytropic relationship, so the isentropic assumption for the temperature was not needed. The polytropic index for helium was kept constant at $n = 1.668$.

The following results are all from the step model with transient heat transfer, polytropic, adiabatic, and isothermal assumptions, at an operating frequency of 1 Hz. The p-V diagram for the step model for all assumptions is shown in Figure 4-2. The p-V diagram of the transient heat transfer model shows that all models start with the same initial conditions at the

maximum volume, and then the transient model converges to a higher pressure and temperature.

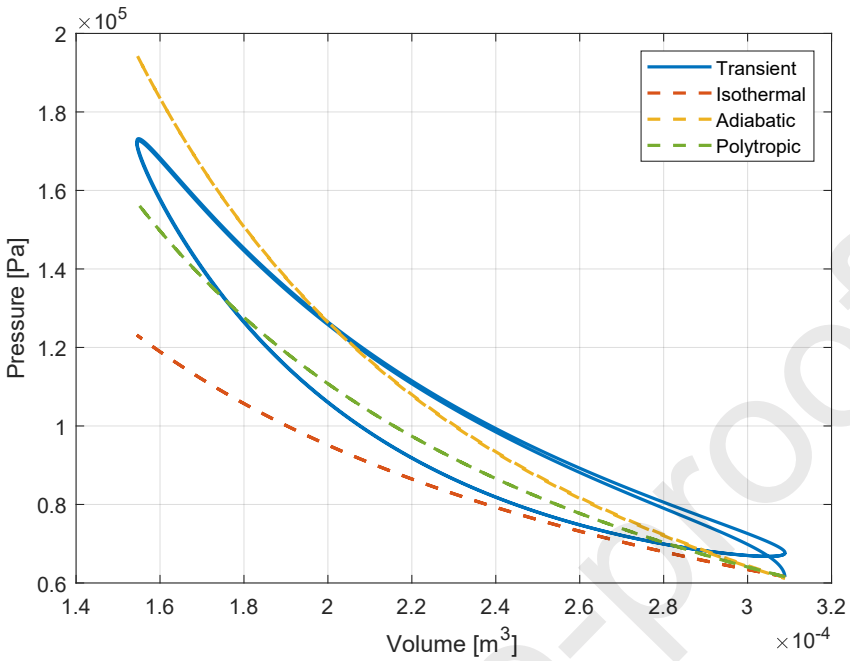

Figure 4-2: p-V diagrams for step model with transient heat transfer, polytropic, adiabatic, and isothermal assumptions

4.1 The Time-Dependence of Heat Transfer

The only p-V diagram in Figure 4-2 with a difference between the compression and expansion processes, and therefore an enclosed area, is the model with transient heat transfer. A phase shift is therefore only present in the transient heat transfer model, as shown in Figure 4-3.

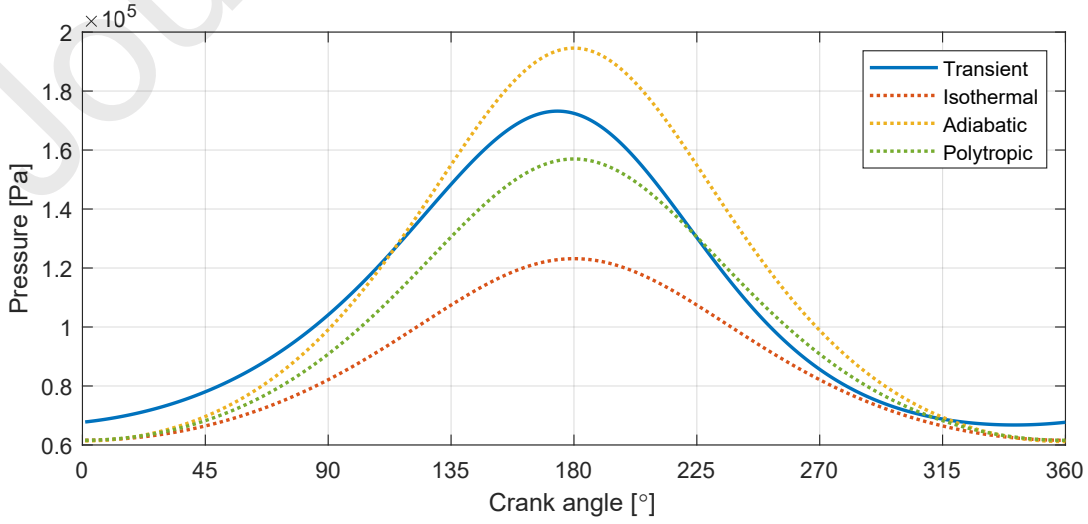

Figure 4-3: Pressure vs crank angle for transient heat transfer, polytropic, adiabatic, and isothermal assumptions

The difference between the polytropic assumption and the transient heat transfer assumption is how the latter takes into consideration the time required for heat transfer to take place, which leads to a phase shift in heat transfer that increases with frequency. While the polytropic assumption still assumes there is heat transfer, this heat transfer is perfectly in phase with the p-V work input. This can be seen in Figure 4-4. This lag in heat transfer is what causes the pressure and temperature to peak before the piston reaches the top dead centre, therefore leading to the pressure phase shift.

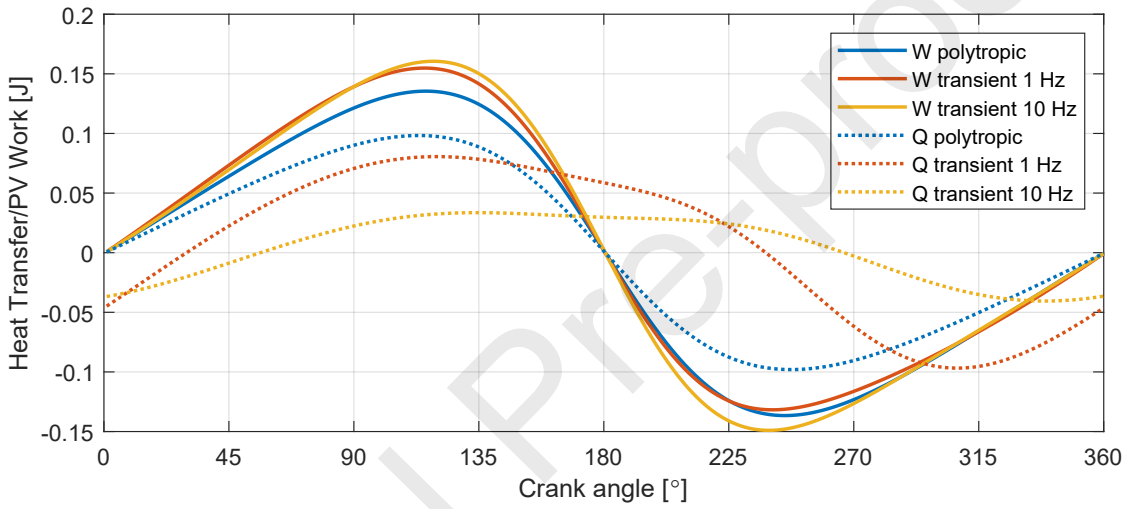

Figure 4-4: Polytropic and transient cyclic p-V work and heat transfer in the step model for 1 Hz and 10 Hz

This simplistic model predicts net heat transfer, which in a single space is hysteresis loss. The only assumption which predicts net heat transfer is one where the heat transfer lags the p-V work, which indicates that the time-dependence of heat transfer is what causes the difference between the compression and expansion work. Since this model is simplistic in that it only contains the fundamental thermodynamic relationships, it can be concluded that the resulting pressure phase shift is purely a result of the relationships between gas properties and the conversions between work, heat, and internal energy.

5 The Pressure Phase Shift using the Schmidt Equations

The Schmidt theory does not explicitly give an equation for the pressure phase shift. However, ϕ can be derived by finding the total volume phase shift and the relationships given for the Schmidt theory defined angles at which the pressure is minimum and maximum. The derived total volume, V_t, can be found by using the Schmidt equations, Equations 1 and 2. It results in an addition of two cosine waves, shown in Equation 15:

$$V_t = V_e + V_c = \frac{1}{2}V_E(1+\kappa) + \frac{1}{2}\kappa V_E(\cos(\theta) + \cos(\theta-\beta)) \quad \text{Equation 15}$$

Adding these two cosine waves and finding the resulting mean, amplitude, and phase shift of the total volume gives:

$$V_t = V_{t,mean} + V_{t,amplitude}\cos(\theta + \phi_{V_t}) \quad \text{Equation 16}$$

Where:

$$V_{t,mean} = \frac{1}{2}V_E(1+\kappa) \quad \text{Equation 17}$$

$$V_{t,amplitude} = \frac{1}{2}V_E\sqrt{\kappa^2 + 1 + 2\kappa\cos(\beta)} \quad \text{Equation 18}$$

$$\phi_{V_t} = \tan^{-1}\left(\frac{-\kappa\sin(\beta)}{1+\kappa\cos(\beta)}\right) \quad \text{Equation 19}$$

The angle where volume is maximum, $\theta_{V_{max}}$, is located at $\theta = -\phi_{V_t}$.

The Schmidt theory defines that the pressure is minimum where $\theta = \theta_{p_{min}}$ (Walker, 1983):

$$\theta_{p_{min}} = \tan^{-1}\left(\frac{\kappa\sin(\beta)}{\tau+\kappa\cos(\beta)}\right) \quad \text{Equation 20}$$

The difference between $\theta_{V_{max}}$ and $\theta_{p_{min}}$ is therefore the phase shift of the pressure in relation to total volume, ϕ:

$$\phi = \theta_{V_{max}} - \theta_{p_{min}}$$

$$\phi = -\left[tan^{-1}\left(\frac{-\kappa\, sin(\beta)}{1+\kappa\, cos(\beta)}\right) + tan^{-1}\left(\frac{\kappa\, sin(\beta)}{\tau+\kappa\, cos(\beta)}\right)\right] \quad \text{Equation 21}$$

It can be seen that for the Schmidt equations, the pressure phase shift is purely based on β, the angle that the expansion space volume variation leads the compression space, κ, the swept volume ratio, and τ, the temperature ratio. This does not take into consideration any losses or heat transfer which could also affect the pressure phase shift. Setting Equation 21 to equal zero leads to κ and β becoming redundant, leaving $\tau = 1$. This means for an ideal Stirling cycle with sinusoidal motion, when $\tau = 1$, there is no net p-V work.

6 Conclusion

This study built a more conclusive picture on how the pressure phase shift manifests with idealising assumptions in a Stirling refrigerator, to better understand its relationship with the net p-V work. An explanation for the hysteresis is given from cyclic heat transfer. Heat transfer peaks just before the end of the expansion and compression processes, causing the pressure to reach a minimum or maximum, respectively, just before the volume does. This is the pressure phase shift. From these relationships, it could be argued that the focus should not be on defining it simply as a loss, but rather as the mechanism which links net heat transfer and net P-V work.

It was found from the transient step model that even though compression and expansion can be modelled as a polytropic process, there will not be a pressure phase shift and any net heat out (and therefore net P-V work required) unless the heat transfer lags the input P-V work. The heat transfer only had this lag when using the transient heat transfer equation, showing that as heat transfer realistically depends on the time available for it to occur, the phase lag of heat transfer and therefore pressure phase shift and net heat loss are due to this time-dependence.

The Schmidt equations were extended to find the conditions that the pressure phase shift would be zero. Even with this ideal analysis, the only time the pressure phase shift is ever zero

is when the temperature ratio, the ratio of the heat source to heat sink temperature, is 1. This means that there must be a non-zero pressure phase shift for any refrigeration effect to occur.

Even though a refrigerator may be working perfectly at a Carnot COP with no losses, there is still a net heat transfer between the gas and its surroundings required to create the refrigeration effect, and therefore a net p-V work input. It then follows that, even during completely ideal operation, there will always be a pressure phase shift due to heat transfer between the gas and the walls and heat exchangers. This shows that anything affecting the net p-V work affects the pressure phase shift, not just what is viewed as 'hysteresis loss'.

Bibliography

Bird, R. B., Stewart, W. E., & Lightfoot, E. N. (1960). *Transport Phenomena*. John Wiley & Sons.

Carslaw, H. S., & Jaeger, J. C. (1959). *Conduction of Heat in Solids*. Clarendon Press.

Chafe, J. N. (1988). *A Study of Gas Spring Heat Transfer in Reciprocating Cryogenic Machinery* Massachusetts Institute of Technology]. Massachusetts, USA.

Chen, N. C. J., & Griffin, F. P. (1983). *A review of Stirling engine mathematical models*. O. R. N. Laboratory.

Gedeon, D. (2016). Sage User's Guide. In. Athens, USA: Gedeon Associates.

Haywood, D. (2004). *Investigation of Stirling-Type Heat-Pump and Refrigerator Systems Using Air as the Refrigerant* University of Canterbury]. Christchurch.

Kornhauser, A. A. (1989). *Gas-Wall Heat Transfer During Compression and Expansion* [PhD, Massachusetts Institute of Technology]. Massachusetts, USA.

Kornhauser, A. A., & Smith, J. L. (1987). A Comparison of Cylinder Heat Transfer Expressions Based on Prediction of Gas Spring Hysteresis Loss. *Fluid Flow and Heat Transfer in Reciprocating Machinery, ASME*.

Kornhauser, A. A., & Smith, J. L. (1993). The Effects of Heat Transfer on Gas Spring Performance. *Journal of Energy Resources Technology*, *115*, 70-75.

Lee, K. P., Smith, J. L., & Faulkner, H. B. (1980). Performance loss due to transient heat transfer in the cylinders of Stirling engines. 15th Intersociety Energy Conversion Engineering Conference, Seattle, Washington.

Martini, W. R. (1983). *Stirling Engine Design Manual* (Second ed.). U.S. Department of Energy

Park, J. S., & Chang, H.-M. (1997). A Stirling Cycle Analysis with Gas-Wall Heat Transfer in Compressor and Expander. In R. G. Ross (Ed.), *Cryocoolers 9* (pp. 147-156). Springer US. https://doi.org/10.1007/978-1-4615-5869-9_18

Pourmovahed, A., & Otis, D. R. (1984). Effects of Thermal Damping on the Dynamic Response of a Hydraulic Motor-Accumulator System. *Journal of Dynamic Systems, Measurement, and Control*, *106*, 21-26.

Scheck, C. G. (1988). *Thermal Hysteresis Loss in Gas Springs* Ohio University]. Ohio, USA.

Schmidt, G. (1871). Theorie der Lehmannschen calorischen maschine. *Zeitschrift des Vereines Deutscher Ingenieure*, *15*.

Stirling Ultracold. (2018). *Stirling Solutions*. Retrieved July 8 2018 from www.stirlingultracold.com/stirling-solutions/

Urieli, I. (1983). A current review of the Stirling cycle machine analysis methods. *Proceedings of the 18th Intersociety Energy Conversion Engineering Conference*, *2*, 702-707.

Urieli, I., & Berchowitz, D. M. (1984). *Stirling Cycle Engine Analysis*. Adam Hilger Ltd.

Walker, G. (1983). *Cryocoolers Part 1: Fundamentals*. Plenum Press.

Walker, G., Reader, G., Fauvel, O. R., & Bingham, E. R. (1993). Stirling, near-ambient temperature refrigerators: innovative compact designs. *6th International Stirling Engine Conference*, 327–333.

Walker, G., Reader, G., Fauvel, O. R., & Bingham, E. R. (1994). *The Stirling Alternative: Power systems, Refrigerants and Heat Pumps*. Gordon & Breach Science Publishers.

Wang, A. C.-M. (1988). *Evaluation of gas spring hysteresis losses in Stirling cryocoolers* [ME, Massachusetts Institute of Technology].

West, C. D. (1986). *Principles and applications of Stirling engines*. Van Nostrand Reinhold Company.

Willich, C., Markides, C. N., & White, A., J. (2017). An investigation of heat transfer losses in reciprocating devices. *Applied Thermal Engineering*, *111*, 903-913.

Wurm, J., Kinast, J. A., Roose, T. R., & Staats, W. R. (1991). *Stirling and Vuilleumier heat-pumps*. McGraw Hill, Inc.

Yang, D., & Gschwendtner, M. (2018). *Hysteresis Loss in Near-Ambient Stirling Refrigerators.* 18th International Stirling Engine Conference, Tainan, Taiwan.

Highlights

- Stirling cooler pressure phase shift linked to hysteresis loss, increased p-V work.
- Relationship derived between the pressure phase shift and the net p-V work
- Schmidt equations lead to ideal pressure phase shift with sinusoidal motion.
- A discrete Stirling cycle is found to have an effective phase shift.
- Pressure phase shift not indication of hysteresis, solely proportional to p-V work.

Declaration of interests

☒ The authors declare that they have no known competing financial interests or personal relationships that could have appeared to influence the work reported in this paper.

☐ The authors declare the following financial interests/personal relationships which may be considered as potential competing interests:

During the preparation of this work the author(s) did not use AI or AI assisted technologies in the writing process.